IVS Memorandum 2008-018v01

9 September 2008

"VLBI2010 Analysis Strategies Tested With the PPP Simulator"

Andrea Pany, Jörg Wresnik, Johannes Böhm

VLBI2010 analysis strategies tested with the PPP Simulator

A. Pany, J. Wresnik, J. Böhm

Abstract
The VLBI2010 Monte Carlo simulations as described by Pany et al. 2008, Wrenik et al. 2007 and MacMillan 2007, yield the big advantage of exactly knowing the input to the simulators which is the sum of VLBI's main stochastic error sources, those being tropospheric wet delay, station clock and thermal noise. Assuming the simulation of group delay observables to be realistic, it is thus possible to test various analysis strategies and different parameterizations on their ability of properly modelling these stochastic processes and thus separating the influences of troposphere and clock. The VLBI2010 PPP Simulator (Pany et al. 2008) can handle single stations which makes it a powerful tool for investigations like this. It is possible to test many different strategies in fairly short time, and the simplicity of this approach helps gaining insight in how the choice of parameters like constraints or the length of time segments impact on station position repeatability.
In this memo we present an investigation on the parameterization of zenith wet delay and station clock, using both the classical least squares (Gauss-Markov model) and the Kalman filter version of the PPP Simulator.

1. Introduction

For VLBI2010 PPP simulations, fictitious group delay observables $delay_{group}$ are generated as given by equation (1):

$$delay_{group} = zwd \cdot mf_w(el) + clk + wn, \quad (1)$$

where *zwd* denotes zenith wet delay, mf_w the wet mapping function (which is assumed to be free of error), *el* elevation angle, *clk* stochastic variations of station clock and *wn* white noise. The group delay observables are generated for fictitious VLBI2010 test schedules. The generation of equivalent zenith wet delays follows the strategy proposed by Nilsson et al. (2007). Stochastic fluctuations of station clock are simulated as sum of a random walk and an integrated random walk with power spectral densities corresponding to a specific clock Allan standard deviation (ASD) as proposed by Herring et al. (1990). More details and the source code for zenith wet delay and clock simulation are provided in Böhm et al. (2007). The white noise in (1) is added to account for the thermal noise of the receiving system.
The group delay observables are generated for 25 identical 24h-sessions, i.e. only the random numbers used in the simulation procedure are changed. All 25 realizations are evaluated with the PPP Simulator and thus a sample of output parameters is gained that can be analyzed statistically. The most important statistical value considered is the rms error of 3D station position of each station. This value can be directly compared to results from OCCAM and Calc/Solve simulations. Other statistical values of interest might be the mean rms errors of zenith wet delay and clock post fit residuals.

All investigations presented here were carried out for the VLBI2010 16 station test schedule st16uni_60_12_230X_0_0.skd if not otherwise stated. This schedule was generated by Antony Searle from NRCan (Natural Resources Canada) and is achieving uniform sky coverage over 12 minute intervals, while switching every 60 seconds. For more details about this type of schedules refer to Petrachenko et al. (2008). The turbulent equivalent zenith wet

delays were generated with the Vienna turbulence simulator (Böhm et al. 2007) using the turbulence parameters provided by Tobias Nilsson from Onsala Space Observatory, Sweden. The values for the turbulence parameters are given in the appendix. The stochastic fluctuations of station clock were simulated assuming a clock with an ASD of 1e-14 @ 50 min. A white noise of 4/sqrt(2) ps per station was added what corresponds to the white noise of 4 ps per baseline added for OCCAM and Calc/Solve simulations.

2. PPP with classical least squares

The standard model for the estimation of zenith wet delays are piecewise linear functions, clock is usually modeled as second order polynomial with superimposed piecewise linear functions, and the components of station position are treated as deterministic parameters and are determined once per session.
In the following sections we will present some tests on zenith wet delay parametrization, the impact of the choice of estimation intervals on position repeatability, the impact of the choice of constraints, and a test on elevation dependent weighting of observations.

2.1 Rapid Gradients

For troposphere delay estimation in real data analysis, McCarthy and Petit (IERS Conventions 2003, 2004) recommend to apply a gradient model, which is given for the wet part of the delay by

$$\Delta L_w = mf_w(el) \cdot \Delta L_w^z + mf_w(el) \cdot \left[G_N \cdot \cos(az) + G_E \cdot \sin(az) \right]. \qquad (2)$$

In (2), ΔL_w is the total wet delay, mf_w the wet mapping function, *el* the elevation angle, ΔL_w^z the zenith wet delay, *az* azimuth, and G_N and G_E denote north and east gradient respectively. Gradients are used to model azimuthal asymmetries in tropospheric wet delays. In real data analysis, gradients are used to model phenomena on long time scales and are thus estimated for time intervals of several hours. Gradient rates are constrained to zero using pretty tight constraints of e.g. 2 mm/24 h. Such phenomena will not exist in the simulated time series of turbulent equivalent zenith wet delays since for VLBI2010 studies only stochastic fluctuations of the wet refractive index are taken into account. However, since turbulence theory provides not only temporal but also spatial correlations of observations, which are used for the generation of turbulent time series, there will be azimuthal asymetries in the simulated time series which cannot be modeled properly with a simple piecewise linear function model. The simulation studies have shown that that the gradient model as given by (2) can partly model these fast asymmetric fluctuations when estimating the gradients for short time segments of a couple of minutes. Figure 1 shows rms position error for a run with the simple piecewise linear functions model (i.e. without estimating gradients), a run with gradients estimated over 12 h time segments (constraints: 2 mm/h), and a run with gradients estimated over 6 min time segments (constraints: 2 mm/h). The same time series of turbulent equivalent zenith wet delays, station clock and white noise were used for the three runs to make sure that differences are only due to the application of the gradient model and to the choice of the time segment for which the gradients are estimated. In Figure 1, the stations are ordered from North to South. The improvement in position repeatability when using rapid gradients is obvious, especially for stations with rather wet tropospheres, i.e. stations with low latitudes (the equator is located between stations KW and FT).

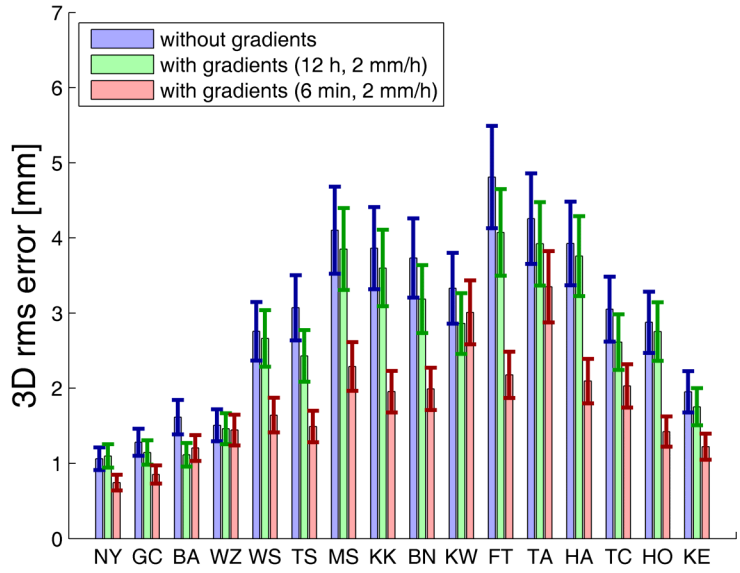

Figure 1: 3D rms error for a run without estimation of gradients (blue), gradients estimated for 12 hour time segments (green), and gradients estimated for 6 min time segments (red) (constraints for gradients: 2 mm/h in both cases). Zwd: 6 min, 48 mm/h; clk: 1 h, 54 mm/h; schedule: st16uni_60_12_230X_0_0.skd; ASD 1e-14 @ 50 min; wn = 4/sqrt(2) ps. The order of stations is from North to South with the equator being located between stations KW and FT. The error bars show 1 sigma of the scatter, i.e. rms/√(2·25).

Figure 2 shows the improvement in percent that was obtained by applying 12 h gradients (left) and 6 min gradients (right).

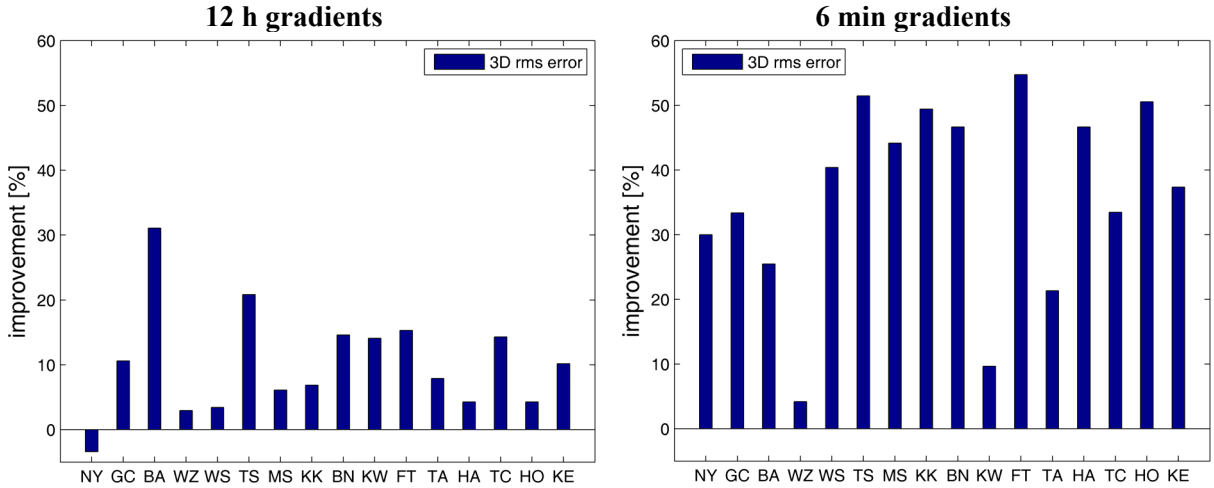

Figure 2: Improvement in 3D rms error in % when applying gradients (left plot: 12 h gradients, right plot: 6 min gradients).

2.2 Varying the length of estimation intervals

To assess the impact of the length of estimation intervals of zenith wet delay, gradients, and clock, the length of estimation interval for one of these parameters was varied, while keeping the other values constant. If not being varied, the estimation intervals where chosen as follows: zwd – 6 min, constrained with 48 mm/h; grd – 6 min, constrained with 2 mm/h; clk – 1 h, constrained with 54 mm/h. When varying the length of estimation intervals, the constraints of gradient rates were kept fixed, while the constraints of zenith wet delay and clock rates were adapted as described in Section 2.3.

2.2.1 Varying the length of estimation intervals for the zenith wet delay

Figure 3 shows 3D rms error (upper plots), mean rms of zenith wet delay post fit residuals (middle plots), and mean rms of clock post fit residuals (lower plots) for simulations where different zenith wet delay estimation intervals were used. It can be seen that the impact on mean rms of clock residuals is small. Rms of zenith wet delay residuals are getting worse for dry stations when using shorter estimation intervals, but there is a significant improvement for wet stations. The improvement in 3D rms is not that clear, but reducing the estimation interval of zenith wet delays from 1 h to 6 min, yields an improvement in 3D rms for all but one stations (see Figure 6, upper left, Section 2.2.4).

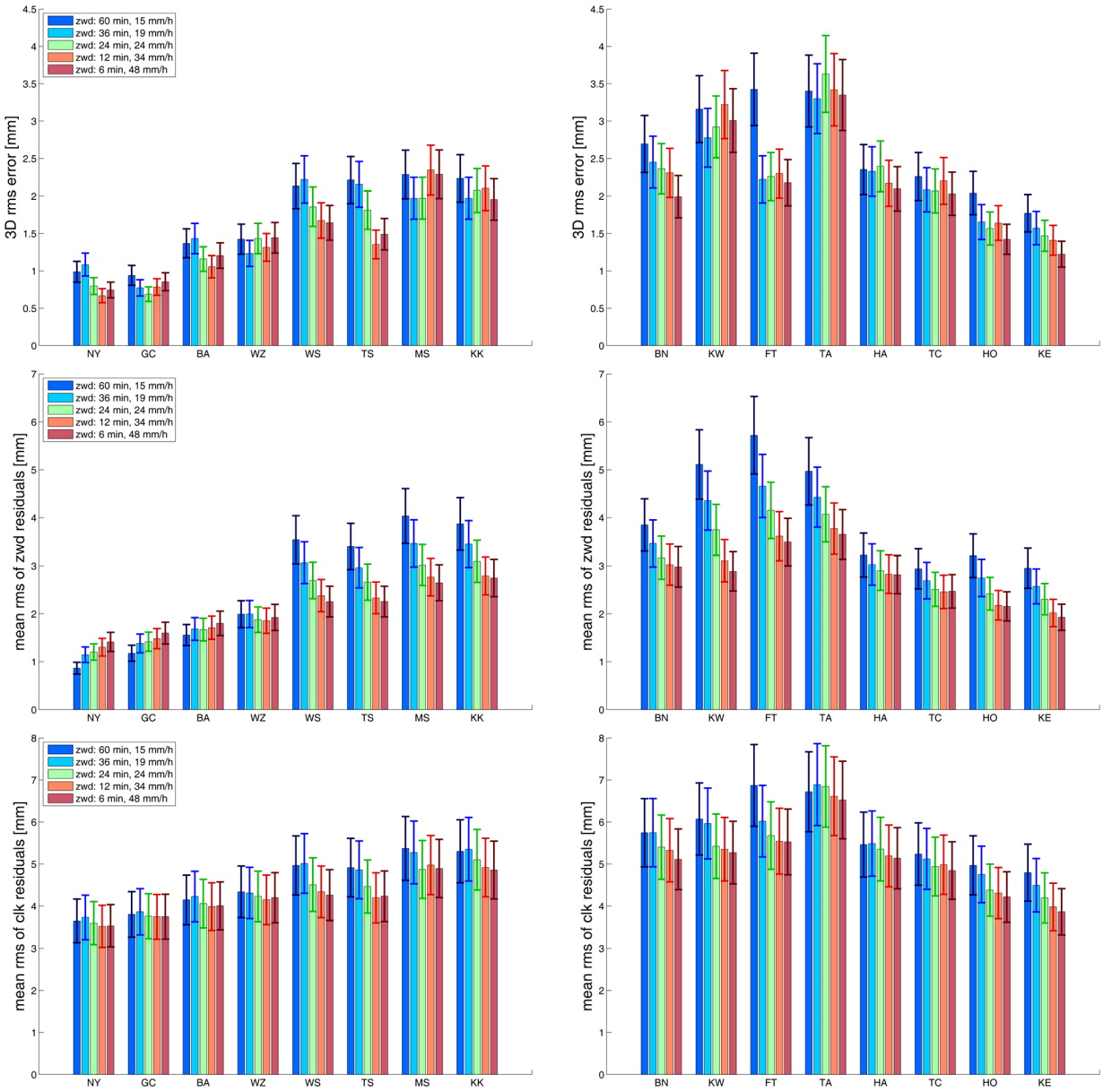

Figure 3: 3D rms error (top), mean rms of zwd post fit residuals (middle) and mean rms of clk post fit residuals (bottom) for different lengths of estimation intervals for zwd. Grd: 6 min, 2 mm/h, clk: 1 h, 54 mm/h; schedule: st16uni_60_12_230X_0_0.skd; ASD 1e-14 @ 50 min; wn = 4/sqrt(2) ps. The order of stations is from North to South with the equator being located between stations KW and FT. The error bars show 1 sigma of the scatter, i.e. rms/√(2·25).

2.2.2 Varying the length of estimation intervals for the gradients

Figure 4 shows 3D rms error (upper plots), mean rms of zenith wet delay post fit residuals (middle plots), and mean rms of clock post fit residuals (lower plots) for simulations where different gradient estimation intervals were used. The conclusions that can be drawn from the results are the same as for varying the zenith wet delay estimation intervals. The improvement in all three parameters, 3D rms error and mean rms of zentih wet delay and clock post fit residuals can be deduced from the upper right plot in Figure 6 (Section 2.2.4).

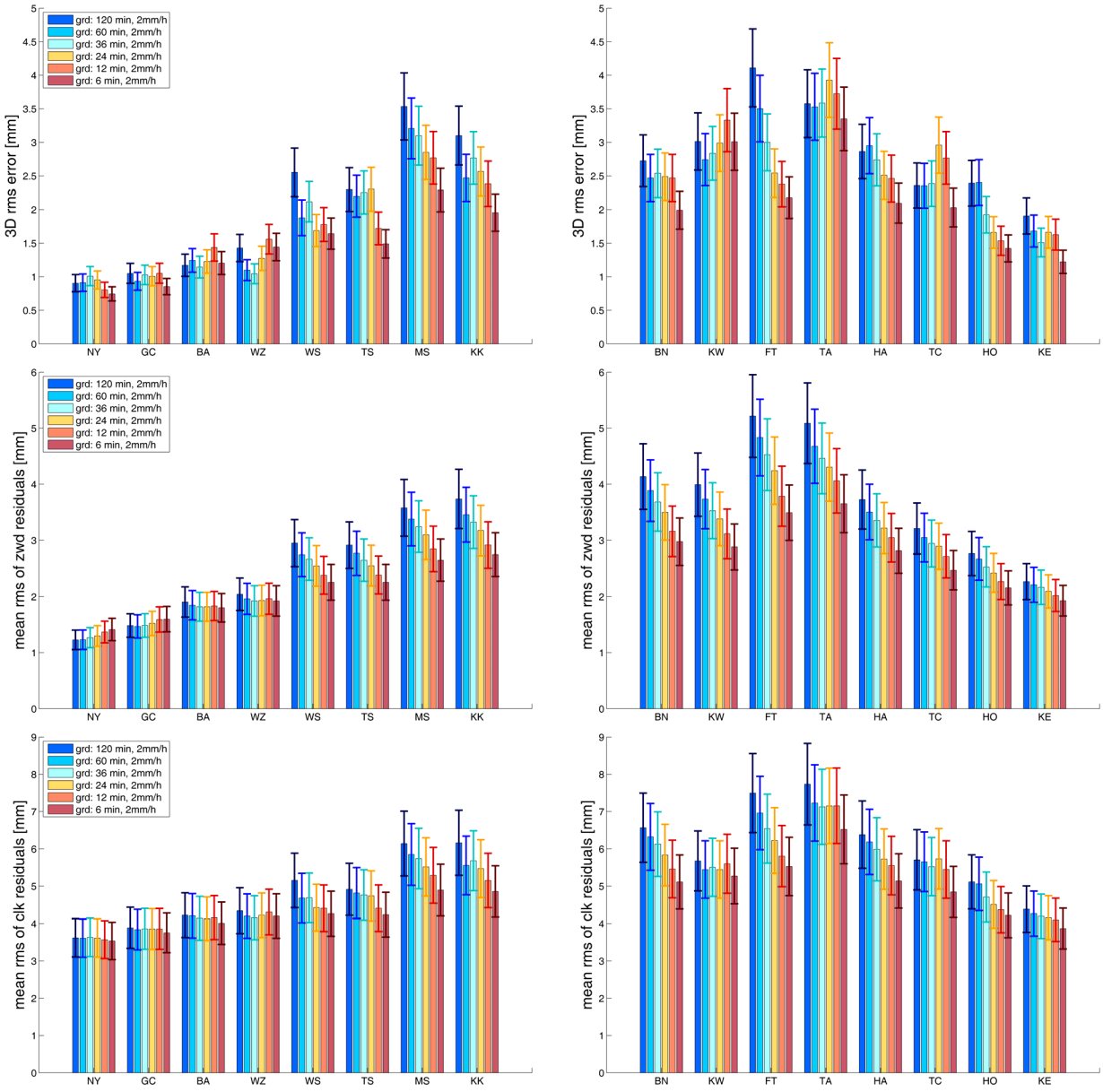

Figure 4: 3D rms error (top), mean rms of zwd post fit residuals (middle) and mean rms of clk post fit residuals (bottom) for different lengths of estimation intervals for grd. Zwd: 6 min, 48 mm/h, clk: 1 h, 54 mm/h; schedule: st16uni_60_12_230X_0_0.skd; ASD 1e-14 @ 50 min; wn = 4/sqrt(2) ps. The order of stations is from North to South with the equator being located between stations KW and FT. The error bars show 1 sigma of the scatter, i.e. rms/√(2·25).

2.2.3 Varying the length of estimation intervals for the clock

Figure 5 shows 3D rms error (upper plots), mean rms of zenith wet delay post fit residuals (middle plots), and mean rms of clock post fit residuals (lower plots) for simulations where different clock estimation intervals were used. In this case, there is a slight improvement for dry stations, when reducing the length of clock estimation intervals but a degradation for wet stations can be observed. The improvement, or degradation respectively, can be deduced from Figure 6 lower left (Section 2.2.4).

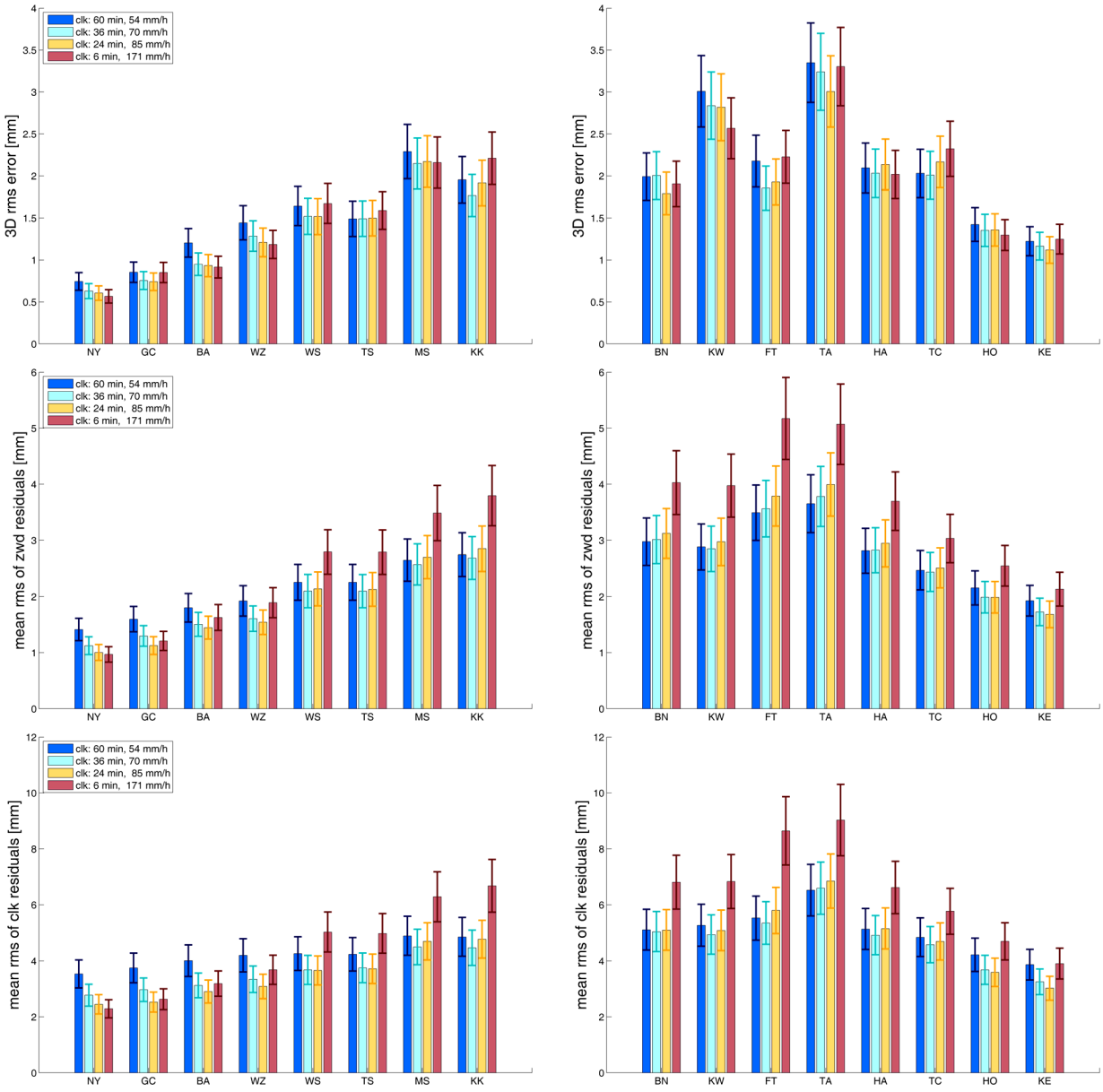

Figure 5: 3D rms error (top), mean rms of zwd post fit residuals (middle) and mean rms of clk post fit residuals (bottom) for different lengths of estimation intervals for clk. Zwd: 6 min, 48 mm/h, grd: 6 min, 2 mm/h; schedule: st16uni_60_12_230X_0_0.skd; ASD 1e-14 @ 50 min; wn = 4/sqrt(2) ps. The order of stations is from North to South with the equator being located between stations KW and FT. The error bars show 1 sigma of the scatter, i.e. rms/√(2·25).

2.2.4 What improvement can be expected using rapid estimates

As a summary of Sections 2.2.1-2.2.3, Figure 6 presents the improvement (or degradation respectively) in 3D rms error (blue), mean rms of zenith wet delay post fit residuals (green), and mean rms of clock post fit residuals that was obtained when reducing the length of estimation interval from 1h to 6 min for one of the parameters to be estimated (zenith wet delay, gradients, clock) while keeping the length of time segments for the other parameters fixed to the values given in the introduction to Section 2.2.
The impact of shorter estimation intervals for zenith wet delays (upper left plot) and gradients (upper right plot), is very similar. Shorter zenith wet delay estimation intervals have slightly more impact on mean rms of zenith wet delay residuals than have shorter gradient time segments. The impact on mean rms of clock residuals and 3D rms errors is almost the same.
The impact of shorter clock estimation intervals looks different. The effect on 3D rms error of wet stations is significantly smaller than is for shorter zenith wet delay or gradient estimation intervals. The impact on zenith wet delay and clock residuals exhibits a strong dependence on the variability of the troposphere but is exactly opposite to the impact of zenith wet delay and gradient estimation intervals: 6 min clocks improve rms errors of zenith wet delay and clocks for dry stations, but significantly degrade it for wet stations.

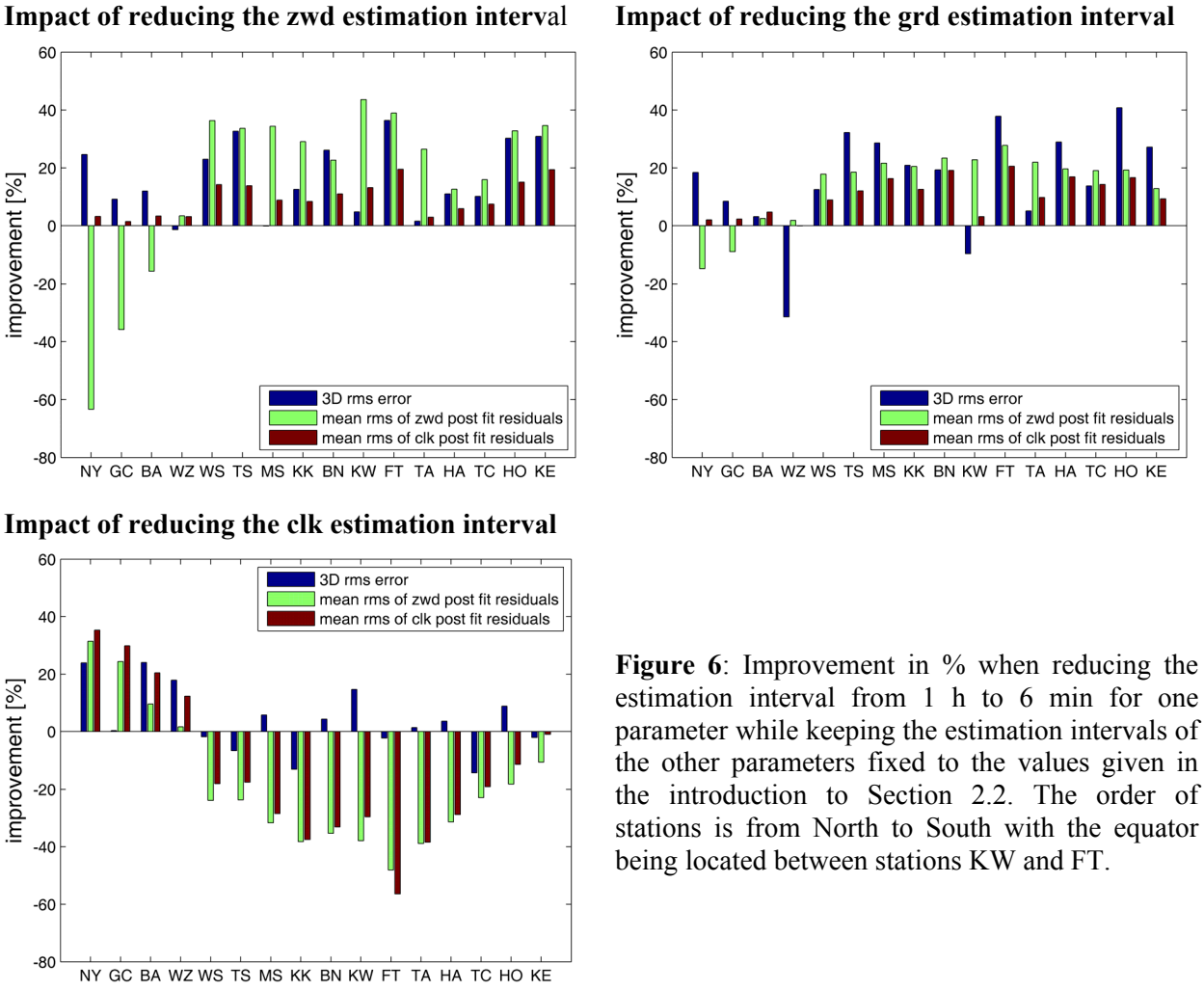

Figure 6: Improvement in % when reducing the estimation interval from 1 h to 6 min for one parameter while keeping the estimation intervals of the other parameters fixed to the values given in the introduction to Section 2.2. The order of stations is from North to South with the equator being located between stations KW and FT.

2.3 Impact of constraints for stochastic parameters on position estimates

The rates of the piecewise linear functions are constrained to zero by introducing pseudo observations. Some tests were carried out to investigate, how the choice of these constraints impacts on position repeatability.
When using 1 hour segments for zenith wet delay estimation (a standard value in real data analysis), a standard value for the constraints is 15 mm/h. This corresponds to the variance rate of 0.7 ps²/s for the Kalman filter used for the OCCAM VLBI2010 simulation studies (Wresnik et al., 2007). When using shorter estimation intervals, e.g. 6 min, the constraints should be adapted as follows:

0.7	ps²/s	| · 60 · 6
252	ps²/6 min	| √
15.875	ps/6 min	| · 60 / 6
158.75	ps/1 h	| · 1e-12 · c · 1e3 (c is the speed of light in m/s)
~ 48 mm/h		

In Figure 7, two analyses with different constraints for zenith wet delay rates are compared. Zenith wet delays and gradients were estimated using 6 min segments. For the clock, 1 h segments were used. Constraints were 2 mm/h for gradient rates, 54 mm/h for clock rates, and 48 mm/h (blue) and 15 mm/h (red) respectively for zenith wet delay rates. Figure 7 shows mean rms of zenith wet delay post fit residuals (upper left), mean rms of clock post fit residuals (upper right), and 3D rms error (lower left). The impact on mean rms of clock residuals is insignificantly small. Mean rms of zenith wet delay residuals show an interesting behavior: at stations with a rather dry troposphere, i.e. high latitude stations, the rms are slightly better when using constraints of 15 mm/h, at stations with a rather wet troposphere, i.e. low latitude stations, the rms are slightly better when using constraints of 48 mm/h. (The stations are ordered from North to South with the equator being located between stations KW and FT). When looking at the 3D rms errors, it is difficult to say, which constraints are better. However, the differences due to varying the zenith wet delay constraints are small.

The situation is similar, when looking at the gradient constraints. For the OCCAM and PPP Kalman Filter simulations, a standard variance rate of 0.5 ps²/s is used for the gradient estimation. This is equal to constraints of roughly 40 mm/h for the gradient rates. Another gradient variance rate tested for the PPP Kalman Filter that gave reasonably good results for this schedule (compare Section 3.2), is 0.015 ps²/s which is equal to about 7 mm/h. For real data analysis, a standard value for the gradient constraints is 2 mm/24 h, which is equal to about 0.08 mm/h, and the standard value normally used for the PPP classical least squares simulations is 2 mm/h. These four values for the gradient rate constraints were tested. The results are shown in Figure 8. The lower left plot presents 3D rms errors, the upper left plot mean rms errors of zenith wet delay post fit residuals and the upper right plot mean rms errors of clock post fit residuals. Looking at the results it can be stated that i) the impact of gradient rate constraints on mean rms of clock post fit residuals is insignificant, ii) the impact on mean rms of zenith wet delay post fit residuals is very small for dry stations, and a little larger, though still small, for wet stations (for wet stations 40 mm/h yield best results), and iii) looking at 3D rms error it is not possible to tell which constraints yield best results.

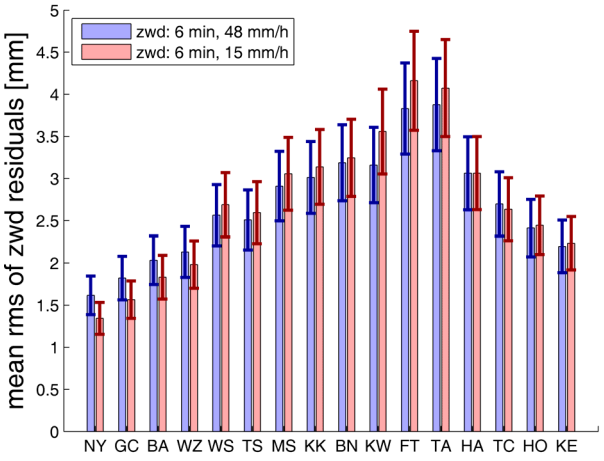

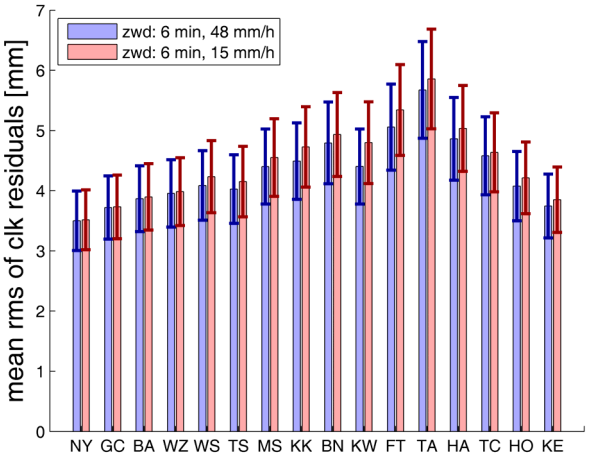

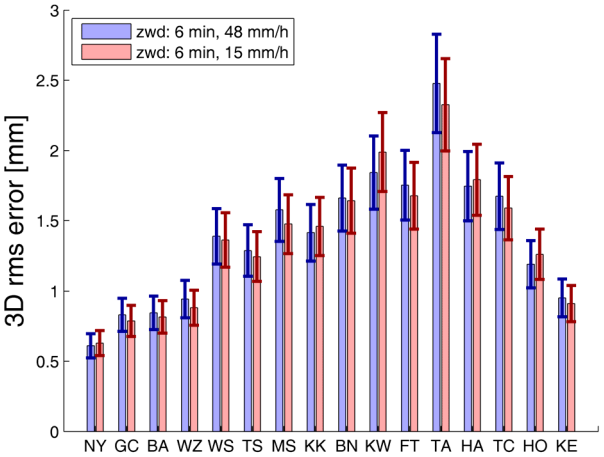

Figure 7: Mean rms of zwd post fit residuals (upper left), mean rms of clk post fit residual (upper right), and 3D rms error (lower left) for two different zwd rate constraints (blue: 48 mm/h, red: 15 mm/h). Zwd: 6 min, 15 and 48 mm/h; grd: 6 min, 2 mm/h; clk: 1 h, 54 mm/h. Elevation dependent weighting as described in Section 2.4 applied. Schedule: st16uni_60_12_230X_0_0.skd; ASD 1e-14 @ 50 min; wn = 4/sqrt(2) ps. The order of stations is from North to South. The error bars show 1 sigma of the scatter, i.e. rms/√(2·25).

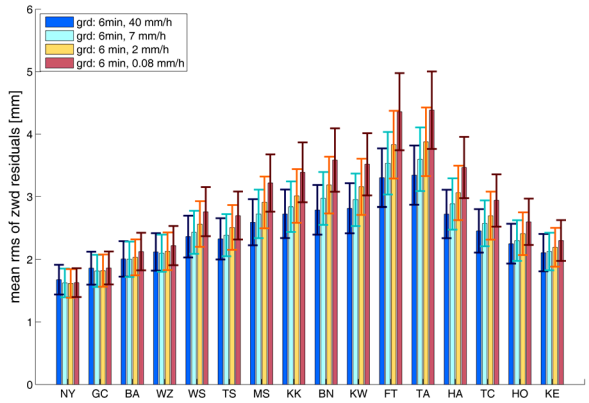

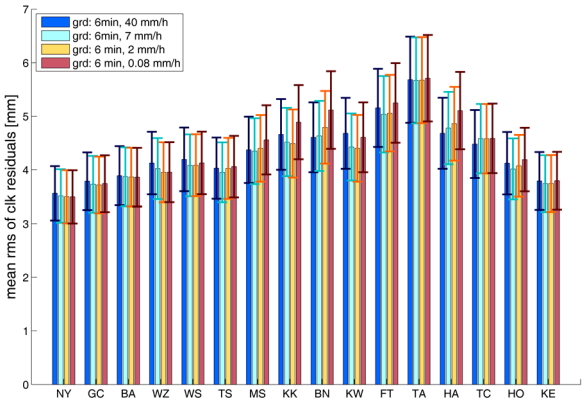

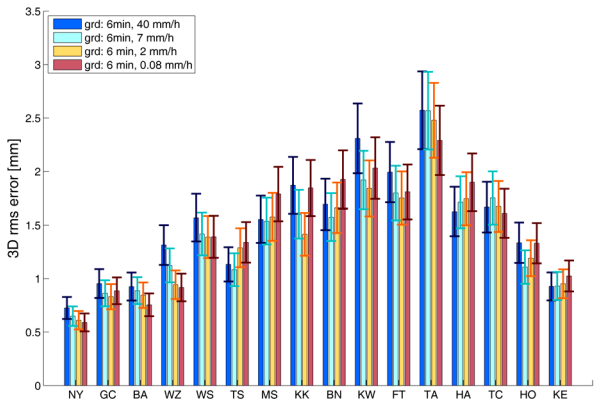

Figure 8: Mean rms of zwd post fit residuals (upper left), mean rms of clk post fit residual (upper right), and 3D rms error (lower left) for four different grd rate constraints (dark blue: 40 mm/h, light blue: 7 mm/h, yellow: 2 mm/h, red: 0.08 mm/h). Zwd: 6 min, 48 mm/h; grd: 6 min, variable constraints; clk: 1 h, 54 mm/h. Elevation dependent weighting as described in Section 2.4 applied. Schedule: st16uni_60_12_230X_0_0.skd; ASD 1e-14 @ 50 min; wn = 4/sqrt(2) ps. The order of stations is from North to South. The error bars show 1 sigma of the scatter, i.e. rms/√(2·25).

A typical value for clock rate constraints in real data analysis is 54 mm/h when using 1 hour time segments. This parameterization is usually used in the VLBI2010 PPP simulations. Constraints could also be determined from the ASD of 1e-14 @ 50 min, which is applied for the simulation of stochastic clock variations:

1e-14	s^2	| ^{2}
1e-18		| · 50 · 60
3e-25	s^2/s	| · 3600
1.08e-21	s^2/h	| √
3.29e-11	s/h	| · 1e-12 · c · 1e3 (c is the speed of light in m/s)
~ 10 mm/h		

Two runs were performed for which the clock was estimated using 1 hour segments and constraints of 54 mm/h and 10 mm/h respectively were applied. (The clock variance rate used for the PPP Kalman Filter (1 ps^2/s) is about 18 mm/h and is thus within the tested range of values.) The results are presented in Figure 9 which shows mean rms of zenith wet delay post fit residuals (upper left), mean rms of clock post fit residuals (upper right), and 3D rms errors (lower left). Comparing the solutions it can be stated that the impact on all parameters is insignificant in the tested range of values.

In conclusion of this Section it can be said that the impact of constraints for all three parameters, zenith wet delay rates, gradient rates, and clock rates, is very small within the tested range of values. Constraints of 48 mm/h for 6 min zenith wet delays, 2 mm/h for 6 min gradient rates, and 54 mm/h for 1 h clocks, are a reasonable choice for the simulation studies.

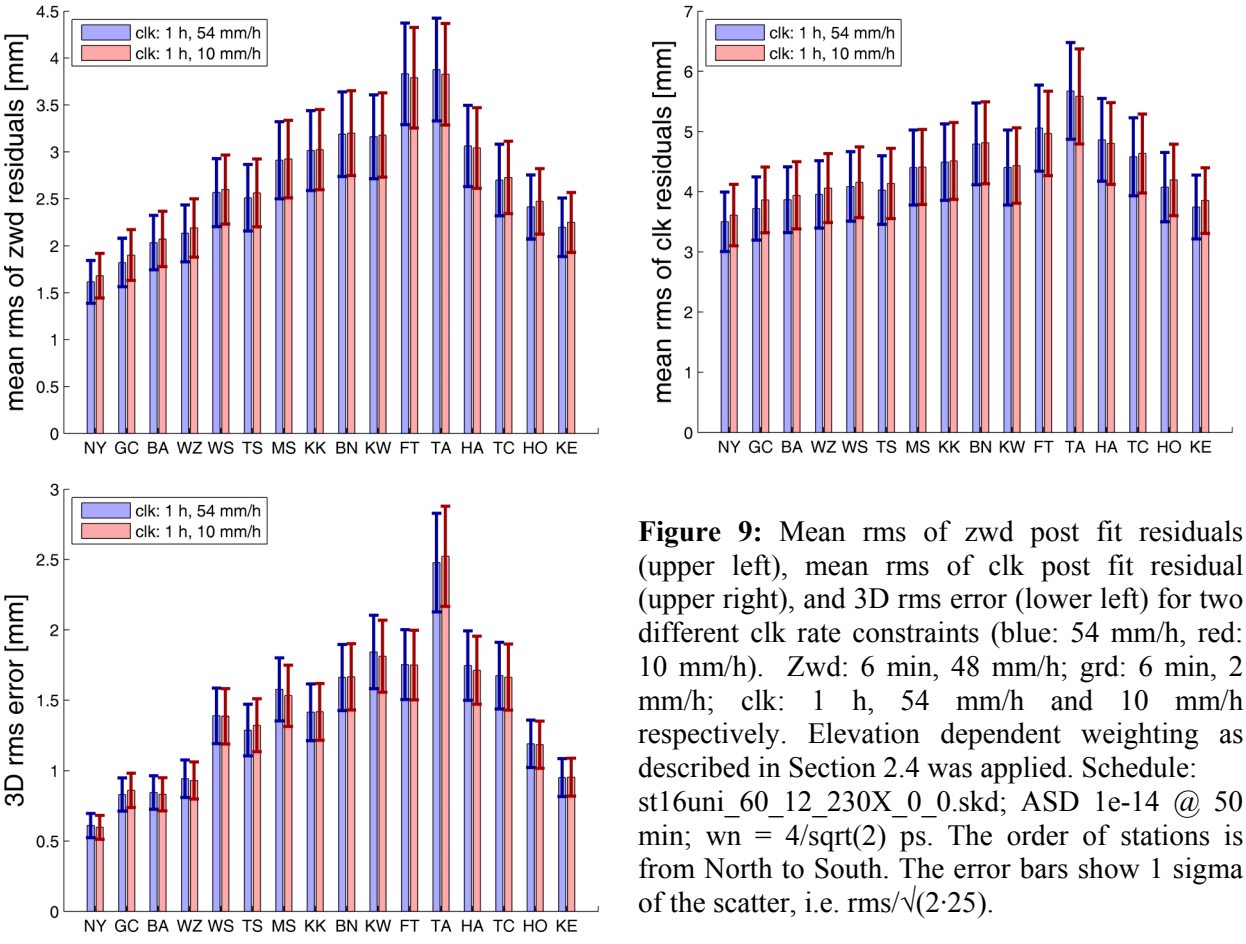

Figure 9: Mean rms of zwd post fit residuals (upper left), mean rms of clk post fit residual (upper right), and 3D rms error (lower left) for two different clk rate constraints (blue: 54 mm/h, red: 10 mm/h). Zwd: 6 min, 48 mm/h; grd: 6 min, 2 mm/h; clk: 1 h, 54 mm/h and 10 mm/h respectively. Elevation dependent weighting as described in Section 2.4 was applied. Schedule: st16uni_60_12_230X_0_0.skd; ASD 1e-14 @ 50 min; wn = 4/sqrt(2) ps. The order of stations is from North to South. The error bars show 1 sigma of the scatter, i.e. rms/√(2·25).

2.4 Elevation dependent weighting of observations

Since the path length a signal has to travel through the atmosphere is increasing with decreasing elevation angle, there will be higher variability of wet delays at lower elevations. Simulation studies have revealed that observations at low elevations quite often show peaks in the zenith wet delay time series that may act like "outliers" tending to bias the piecewise linear functions. A strategy might thus be to weight observations according to their elevation angle. J. Gipson (Gipson, 2007) proposed to add an atmospheric uncertainty to the observation uncertainty:

$$\sigma_w^2(el) = \sigma_{obs}^2 + a \cdot mf(el)^2 , \qquad (3)$$

where σ_w^2 is the weighted observation noise, *el* the elevation angle, σ_{obs}^2 the unweighted observation noise (i.e. $4^2/\mathrm{sqrt}(2)^2$ = 8 ps^2), *mf* the mapping function, and *a* a constant atmospheric noise. Gipson achieved best results using an *a* of ~10 ps. This value was also applied to the PPP simulations. Figure 10 shows a comparison of 3D rms error for a run without the application of elevation dependent weighting (blue) and a run with the application of elevation dependent weighting (red). There is a clear improvement in 3D rms error when applying elevation dependent weighting.

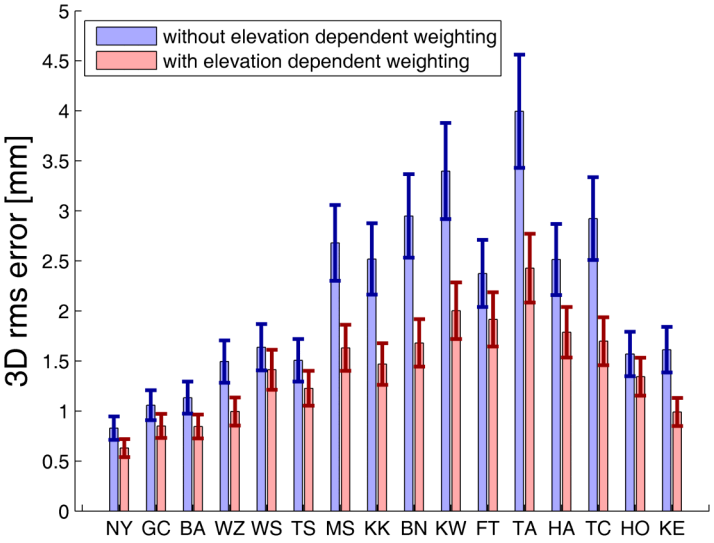

Figure 10: 3D rms error for a run without application of elevation dependent weighting (blue) and a run with application of elevation dependent weighting (red). Zwd: 12 min, 34 mm/h; grd: 12 min, 2 mm/h; clk: 1 h, 54 mm/h; schedule: st16uni_60_12_230X_0_0.skd; ASD 1e-14 @ 50 min; wn = 4/sqrt(2) ps; atmospheric noise: 10 ps. The order of stations is from North to South. The error bars show 1 sigma of the scatter, i.e. rms/√(2·25).

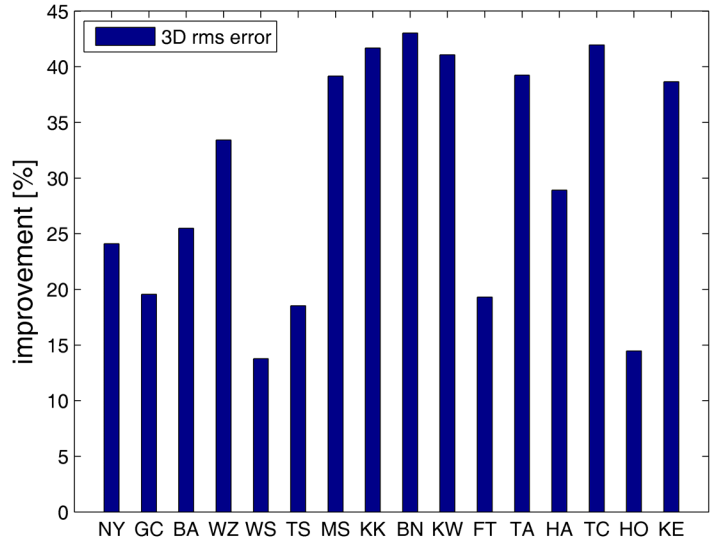

Figure 11: Improvement in 3D rms error in % when applying elevation dependent weighting.

2.5 Spherical harmonics – an outlook

Another approach to zenith wet delay modeling might be to introduce spherical harmonic functions of higher degree and order. Böhm and Schuh (2001) have applied a spherical harmonics model to real data analysis. The approached they used is given by

$$\Delta L_w(el,az) = mf(el)\cdot L_w^z + mf(el)\cdot\cot(el)\cdot SH_{nm}(zd,az) \qquad (4)$$

with ΔL_w denoting the total wet delay, *el* elevation angle, *az* azimuth, *mf* the mapping function, L_w^z the zenith wet delay, SH_{nm} spherical harmonic functions of degree *n* and order *m*, and *zd* zenith distance. Böhm and Schuh tested spherical harmonics of degree n = 1, 2, 3 and order m = 0, 1 as well as different combinations of these spherical harmonic functions. They found a small improvement in terms of height repeatability when using this model instead of the standard gradient model given by (2). However, they estimated the spherical harmonics for 12 h and 6 h time intervals. VLBI2010 analyses, having so many more observations available, might benefit from rapid spherical harmonic estimates of higher degrees and orders. One advantage of spherical harmonic functions might be that they cannot only model asymmetries in azimuthal direction, but that they also yield the possibility of modelling asymmetries in vertical direction. Gradients as used in (2) are similar to spherical harmonic functions of degree and order one:

gradients: $G_N\cos(az) + G_E\sin(az)$ (5a)

SH_{11}: $\left(a_{11}\cos(az) + b_{11}\sin(az)\right)\cdot\left(-\sin(zd(i))\right)$. (5b)

In (5b), a_{11} and b_{11} denote the coefficients of the spherical harmonics functions. The differences of the two approaches are shown in Figure 12 upper left and Figure 12 middle left. In contrast to the gradients, the spherical harmonic functions model is additionally dependent on elevation angle. While the degree *n* of the spherical harmonic functions defines the resolution of the model in elevation, the order *m* defines the resolution in azimuth.

First tests with rapid low order spherical harmonic functions have not revealed a significant improvement. However, spherical harmonic functions of higher degrees and orders might yield the possibility of a better modeling of spatial structures in the troposphere without increasing the number of parameters to be estimated, since only the coefficients a_{nm} and b_{nm} have to be determined. Another possibility might be to use combinations of spherical harmonic functions or spherical harmonic expansions. Although this would mean an increase in the number of parameters to be estimated, the high observation density of VLBI2010 schedules might make this possible too. It is planned to carry out more detailed investigations with this respect.

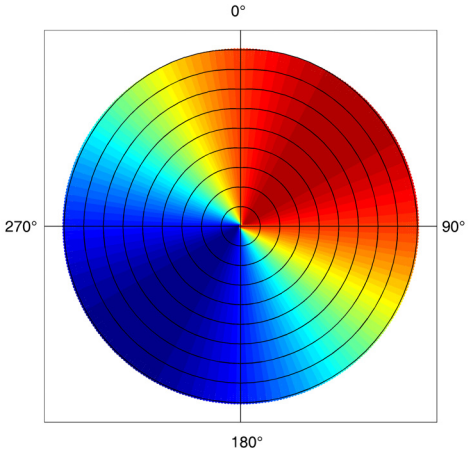

Gradient model: $1 \cdot \cos(az) + 1 \cdot \sin(az)$

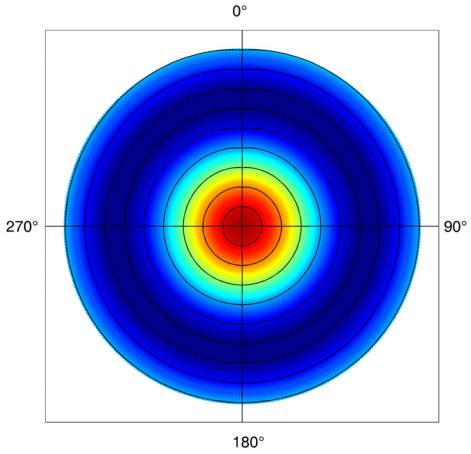

$$SH_{30} = \frac{1}{2}\cos(zd) \cdot \left(5\cos^2(zd) - 3\right) \cdot \left(1 \cdot \cos(az) + 1 \cdot \sin(az)\right)$$

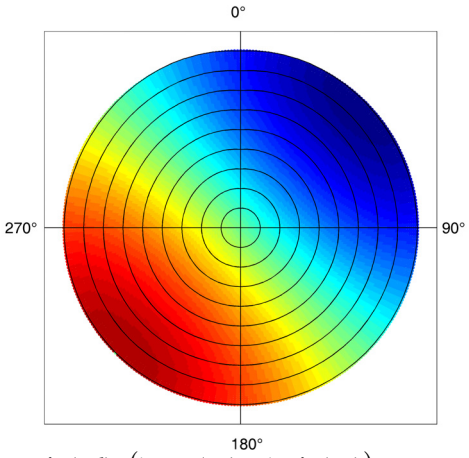

$$SH_{11} = -\sin(zd) \cdot \left(1 \cdot \cos(az) + 1 \cdot \sin(az)\right)$$

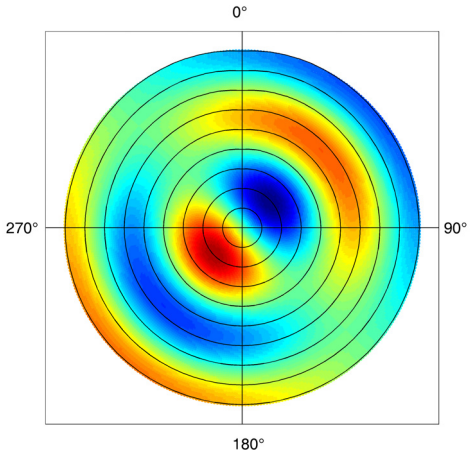

$$SH_{51} = -\frac{15}{8}\sin(zd) \cdot \left(21\cos^4(zd) - 14\cos^2(zd) + 1\right) \cdot \left(1 \cdot \cos(az) + 1 \cdot \sin(az)\right)$$

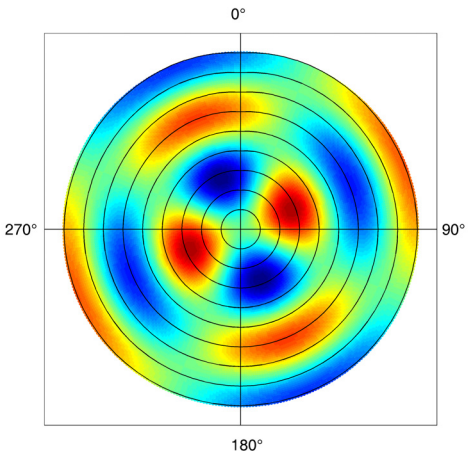

$$SH_{62} = \frac{105}{8}\sin^2(zd) \cdot \left(33\cos^4(zd) - 18\cos^2(zd) + 1\right) \cdot \left(1 \cdot \cos(2 \cdot az) + 1 \cdot \sin(2 \cdot az)\right)$$

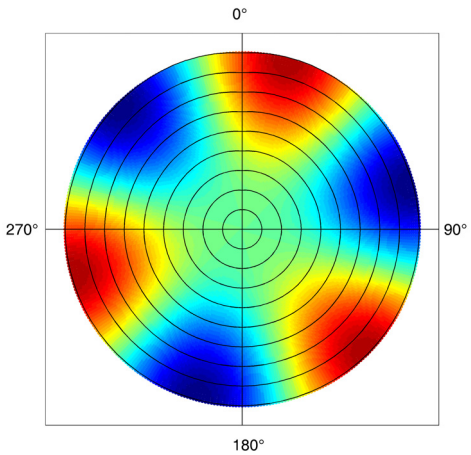

$$SH_{33} = -15\sin^3(zd) \cdot \left(1 \cdot \cos(3 \cdot az) + 1 \cdot \sin(3 \cdot az)\right)$$

Figure 12: Gradient model and spherical harmonics model plotted for a certain time instant with gradients and coefficients being 1. The degree *n* defines the resolution in elevation, the order *m* the resolution in azimuth. Spherical harmonic functions of higher degrees and orders might make it possible to model the spatial structure of the atmosphere for short time periods of several models in more detail than is possible with the classical gradients model.

3. PPP with Kalman filter

In the Kalman filter version of the PPP Simulator, zenith wet delay is treated as stochastic process and modelled as random walk. Zenith wet delay can be superimposed with gradients, which can be treated either as deterministic or as stochastic parameters (Section 3.1). Station clock is also treated as stochastic process and is composed of a deterministic rate superimposed with a random walk offset. Station coordinates are treated as deterministic parameters and are estimated once per session.
The Kalman filter has to be told, how much the stochastic parameters are varying. This is done by giving the variance rates of the stochastic processes. An investigation on the impact of the variance rates of zenith wet delays and gradients was carried out. Results are presented in Section 3.2.
Another strategy to be pursued is to apply elevation dependent weighting of observations within the filtering process. This topic is addressed in Section 3.3.

3.1 Gradients

In the OCCAM Kalman Filter used for real data analysis, it is possible to apply gradients, which are treated as deterministic parameters. As stated in Section 2.1, when speaking about gradients in the context of VLBI2010 simulations, we mean fast azimuthally asymmetric fluctuations of wet refractive index. Since it is likely that deterministic gradients will not suffice to model these short periodic asymmetries, we treated the gradients as random walk processes and compared it to solutions without the application of gradients and the application of deterministic gradients. Results can be seen in Figure 13. The same time series of turbulent equivalent zenith wet delay, station clock and white noise were used for the three runs, differences thus being only due to applying deterministic or random walk gradients. The order of stations in this plot is from North to South. It can be deduced that dry stations (stations in high latitudes) do not benefit from the application of random walk gradients while there is an improvement for rather wet stations (stations with low latitudes). The stations are ordered from North to South, the equator is located between stations KW and FT.

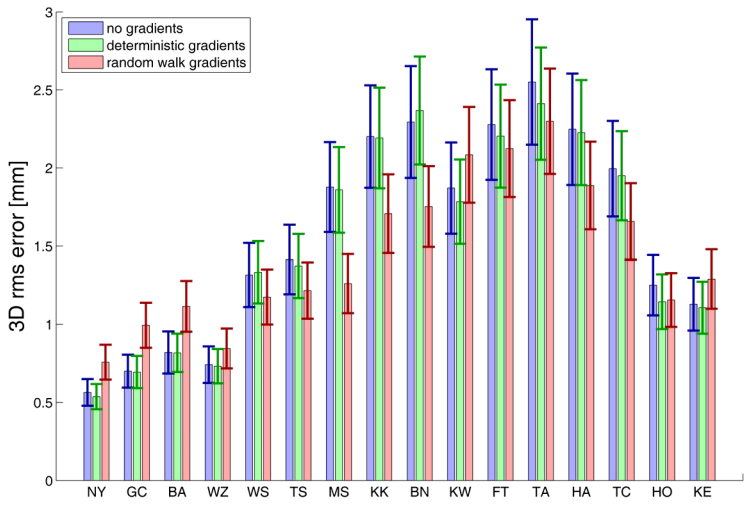

Figure 13: 3D rms error for a run without estimation of gradients (blue), with estimation of deterministic gradients (green), and with estimation of random walk gradients with a variance rate of 0.5 ps²/s (red). Zwd: random walk, 0.7 ps²/s; clk: deterministic rate plus random walk offset, 1 ps²/s; schedule: st16uni_60_12_230X_0_0.skd; ASD 1e-14 @ 50 min; wn = 4/sqrt(2) ps. The order of stations is from North to South. The error bars show 1 sigma of the scatter, i.e. rms/√(2·25).

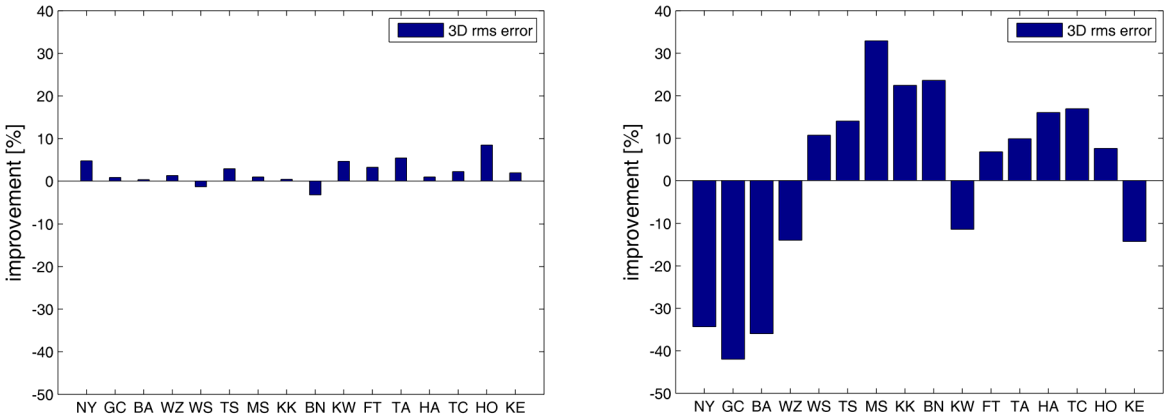

Figure 14: Improvement in 3D rms error in % when applying deterministic (left) or random walk (right) gradients. The order of stations is from North to Sout with the equator being located between stations KW and FT.

Figure 14 presents the improvement in 3D rms error in % that was obtained applying deterministic (left plot) or random walk (right plot) gradients. As can be seen, there is a relativley small improvement for almost all stations when applying deterministic gradients. The effect of applying random walk gradients is much more significant. For dry stations, a significant degradation of 3D rms error can be observed, while for almost all wet stations 3D rms error was improved.

3.2 Variance rates

Variance rates determine how much the stochastic parameters of the model are allowed to vary and their choice is thus an important factor in the estimation of stochastic parameters such as zenith wet delay and station clock. For the VLBI2010 simulations with OCCAM Kalman Filter, an investigation has been carried out with different combinations of zenith wet delay and gradient variance rates in order to determine most suitable values to be applied for all further simulation studies. This investigation was carried out for a different VLBI2010 test schedule, stat16_12_3p5D0ln.skd, produced by J. Gipson from Goddard Space Flight Center (GSFC, Maryland, USA) (Behrend et al., 2007). This type of schedules was generated with the SKED software (Vandenberg, 1999), using the so called “burst mode” (i.e. the data are first buffered and then written to disk, what reduces the on-source time), a new list of radio sources (consisting of 200 of the 230 sources of the list of Leonid Petrov (Petrov, 2007)), and a new scheduling strategy. The best values for the variance rates were found to be 0.7 ps²/s for zenith wet delay and 0.5 ps²/s for gradients (Wresnik et al., 2007). This investigation was carried out with the same combinations of variance rates for the same schedule and in addition for schedule st16uni_60_12_230X_0_0.skd using the PPP Kalman Filter. The time series of turbulent equivalent zenith wet delays for schedule stat16_12_3p5D0ln.skd and were generated using a former set of turbulence parameters. These time series were provided by T. Nilsson from Onsala Space Observatory, Sweden. Results for this investigations are plotted in Figure 15. From these results it can be said that the impact of zenith wet delay and gradient variance rates is very small for most of the stations except for a few stations with rather wet, i.e. highly variable, troposphere. The choice of variance rates of 0.7 ps²/s for zenith wet delays, and of 0.5 ps²/s for gradients, is a reasonable choice for both schedules tested, although the results for schedule st16uni_60_12_230X_0_0.skd might suggest that variance rates of 0.7 and 0.015 ps²/s might eventually be a better choice for this specific schedule.

Looking at these results, it is to suppose that the choice of variance rates might be dependent on i) the variability of the troposphere above a station, and ii) the observation density. Thus,

another investigation was carried for which only one station was analyzed. Time epoch, azimuth, and elevation of station Wettzell (WZ) from two schedules, st16uni_60_12_230X_0_0.skd and st16uni_30_6_230X_0_0.skd, were used to generate 250 24 h sessions for different combinations of turbulence parameters. The latter schedule achieves uniform sky coverage for 6 minute intervals, while switching every 30 seconds (see Petrachenko et al., 2008) for details. The schedule with a switching rate of 60 s has about 69700 observations per session, the schedule with a switching rate of 30 s about 139560.

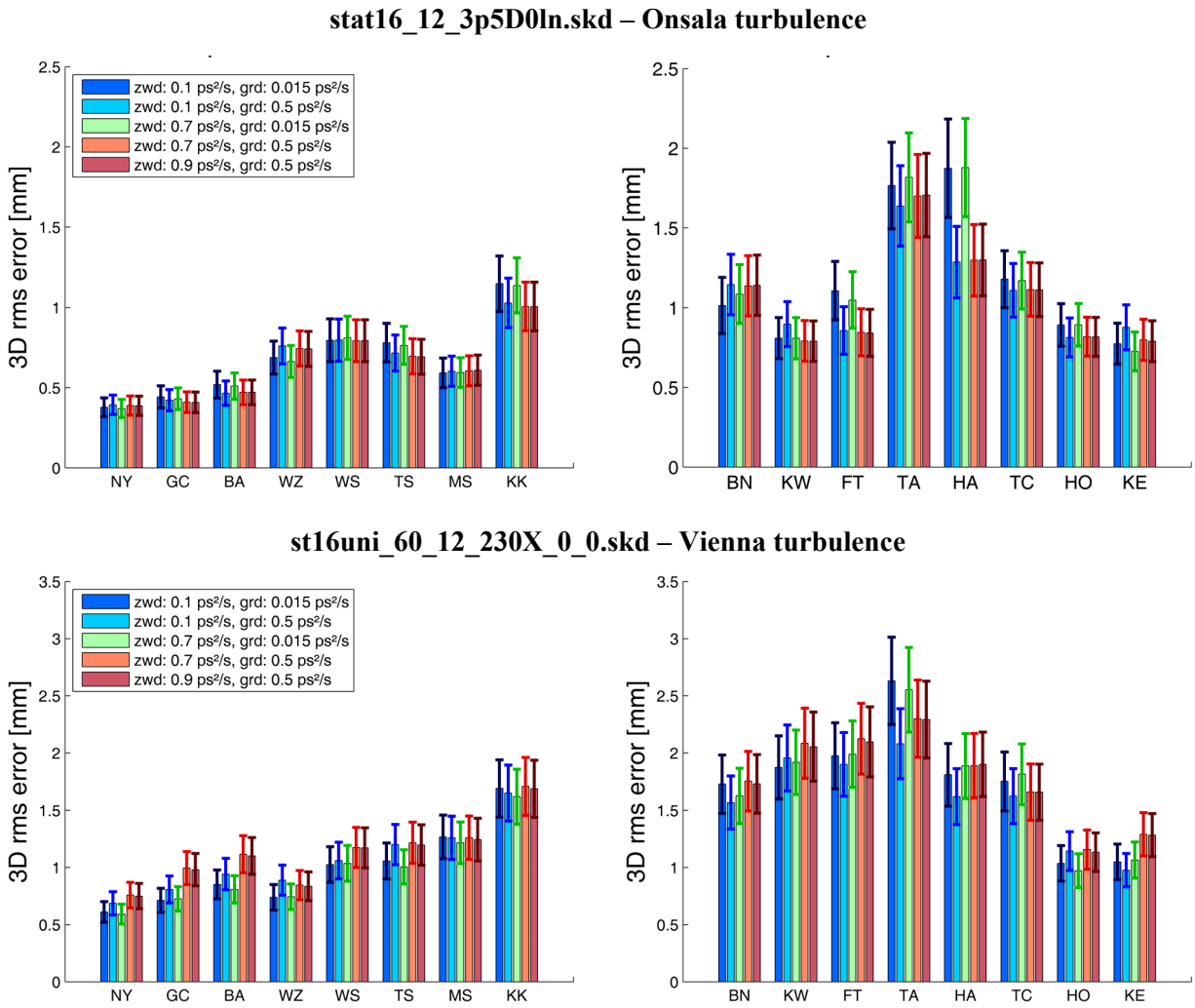

Figure 15: 3D rms error for different combinations of zwd and grd variance rates for schedule stat16_12_3p5D0ln.skd (upper plots) and st16uni_60_12_230X_0_0.skd (lower plots). Variance rate for clk: 1 ps²/s. ASD 1e-14 @ 50 min; wn = 4/√2 ps. The order of stations is from North to South. The error bars show 1 sigma of the scatter, i.e. rms/√(2·25).

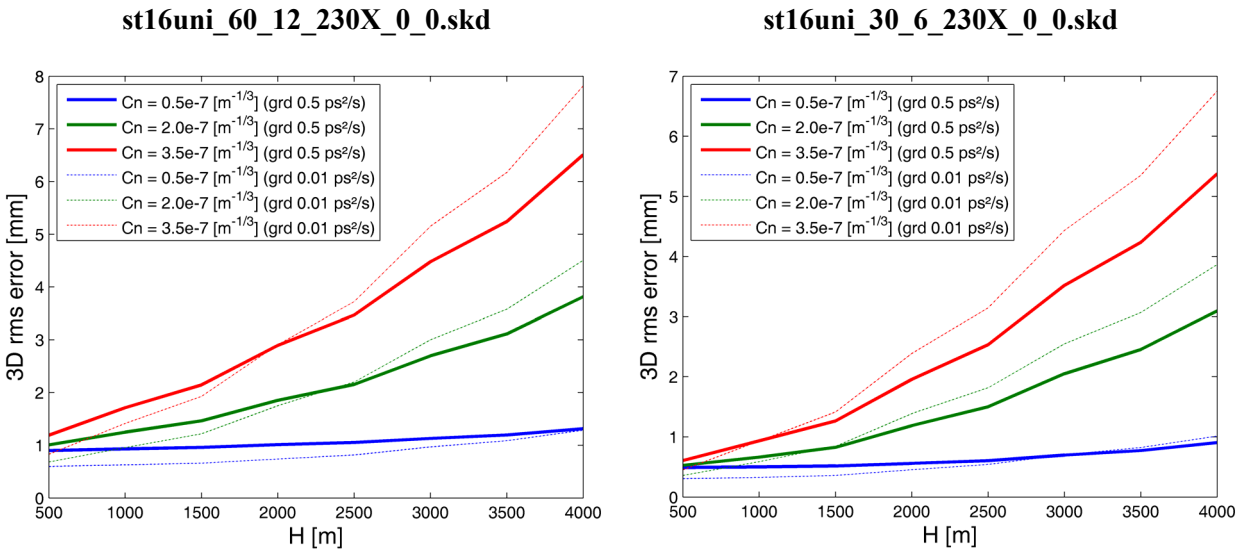

Figure 16: 3D rms error versus effective height H of wet troposphere for station Wettzell for two different schedules. The curves show results for different refractive index structure constants C_n, and two different gradient variance rates (bold lines: 0.5 ps²/s, thin lines: 0.01 ps²/s). Variance rate of zwd: 0.7 ps²/s, variance rate of clock: 1 ps²/s. ASD 1e-14 @ 50 min; wn = 4/√2 ps.

Results are shown in Figure 16 (on the left for the schedule with a switching rate of 60 s, and on the right for the schedule with a switching rate of 30 seconds). The plots show 3D rms error versus effective height H of wet troposphere for different refractive index structure constants C_n and a wind of 7 m/s blowing towards North-East. The solid bold lines show results where a variance rate of 0.5 ps²/s war used for the gradients, the dashed thin lines show results where a variance rate of 0.01 ps²/s was used for the gradient estimation. It can be stated that i) for lower C_n and H values, the smaller variance rates yield better results, while for higher C_n and H values, the larger variance rates yield better results, and ii) for the schedule with the higher observation density (i.e. the one with a switching rate of 30 s), the larger variance rates yield better results already for lower C_n and H values compared to the schedule with less observation density. This shows that the choice of variance rates is indeed dependent on the prevailing atmospheric conditions at a station, as well as on the observation density. However, in the range of turbulence parameters that are used for the VLBI2010 simulations (C_n values are in the range of 0.35e-7 to 3.09e-7 $m^{-1/3}$, H values in the range of 1322 to 2569 m), the differences in 3D rms error due to the choice of variance rates for the gradients are small.

3.3 Elevation dependent weighting

For the same reasons explained in Section 2.4, elevation dependent weighting was applied to the Kalman filter solution. The weighting was performed using Equation (3) (Section 2.4). Figure 17 shows 3D rms error for a run without elevation dependent weighting (blue) and a run with elevation dependent weighting (red). It can be seen that elevation dependent weighting improves 3D rms error for all stations. It should be mentioned that with the OCCAM Kalman Filter no such improvement could be observed. However, the stochastic model of the OCCAM Kalman Filter is more sophisticated and performs a downweighting as soon as the difference of prediction and measurement in the filter process is too large. Since this will be the case especially for observations at low elevations, this might be an explanation for the fact that elevation dependent weighting does not improve results for the OCCAM Kalman Filter.

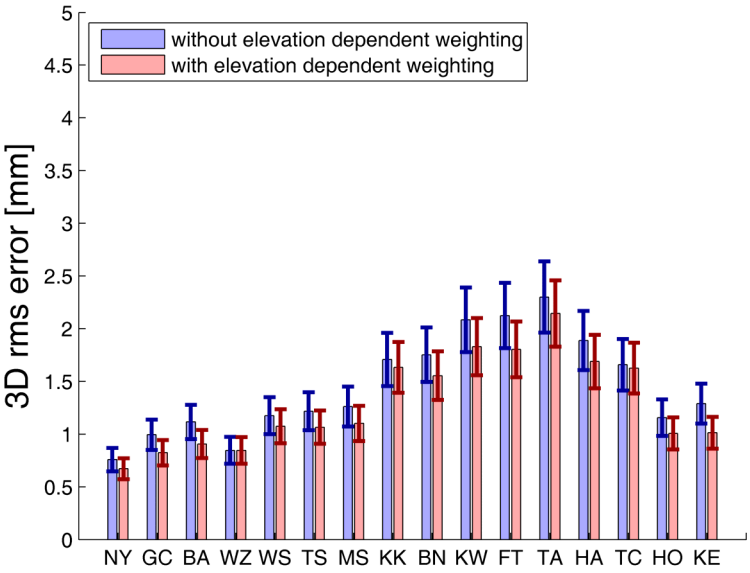

Figure 17: 3D rms error for a run without elevation dependent weighting (blue), and a run with elevation dependent weighting applied (red). Zwd: random walk, 0.7 ps²/s; grd: random walk, 0.5 ps²/s; clk: deterministic rate plus random walk offset, 1 ps²/s; atmospheric noise applied for elevation dependent weighting: 10 ps; schedule: st16uni_60_12_230X_0_0.skd; ASD 1e-14 @ 50 min; wn = 4/sqrt(2) ps. The order of stations is from North to South. The error bars show 1 sigma of the scatter, i.e. rms/√(2·25).

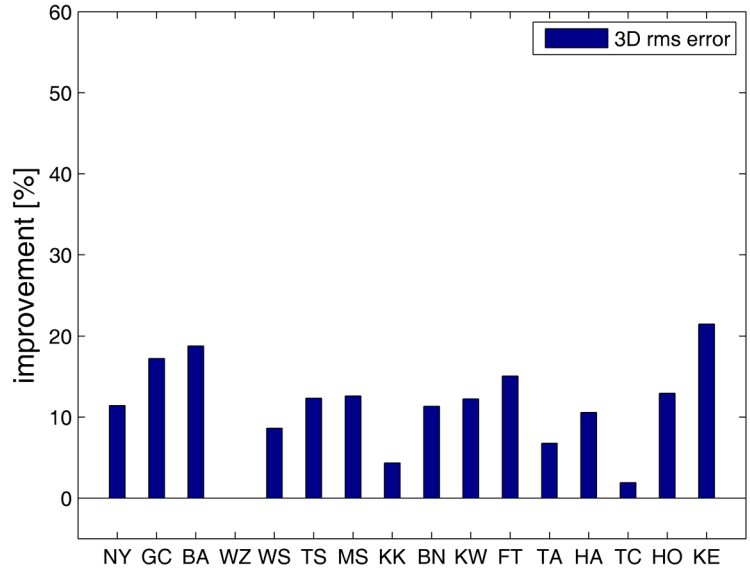

Figure 18: improvement of 3D rms error when applying elevation dependent weighting in %.

4. Limitations

The PPP Simulator, mainly due to its simplicity, has proven to be a powerful tool for VLBI2010 simulation studies. However, it has to be kept in mind that it performs a PPP solution and no network solution as the OCCAM and Calc/Solve simulators do. Although comparisons of PPP Kalman Filter results to OCCAM Kalman Filter results have shown a good agreement, the PPP results only give an indication of what strategy might yield an improvement. What is good for PPP might as well not yield any significant improvement for network solutions. Furthermore, the stochastic model of the PPP Simulator is not as sophisticated as are the stochastic models of OCCAM and Calc/Solve.

There is some scatter in 3D rms error which is mainly reflecting the variability of the troposphere. Theoretically, the biases of Up, North and East component (i.e. the mean over the 25 residuals for each component) should be zero. In practice however, since only 25 repetitions are performed, this will not be the case. Figure 19 shows height biases for all 16 stations. The plot shows results of a run with the classical least squares method (blue - zwd: 6

min, 48 mm/h; grd: 6 min, 2mm/h; clk: 1 h, 54 mm/h), and of a run with the PPP Kalman filter (red - zwd: random walk, 0.7 ps²/s; grd: random walk, 0.5 ps²/s; clk: deterministic rate plus random walk offset, 1 ps²/s). The error bars show 1 sigma of the bias, i.e. scatter/√25. For both methods the same input time series were used. The biases for North and East component are significantly smaller (almost zero) than the height biases.

Since the scatter of the 3D rms error, i.e. the scatter of height, North, and East residuals, is mainly dependent on the variability of the troposphere, it is likely, that also the absolute value of the bias will be sensitive to the turbulence parameters. Figure 20 shows height biases for station WZ for schedule st16uni_60_12_230X_0_0.skd (using PPP Kalman filter). In this case, 250 repetitions were used and the turbulence parameters were varied. The plot on the right shows height biases versus effective height of wet troposphere for C_n values of 0.5e-7, 2.0e-7 and 3.5e-7 $m^{-1/3}$ and a wind of 7 m/s blowing towards North-East. The plot on the left shows the run with a C_n of 2.0e-7 $m^{-1/3}$ but with error bars (scatter/√25) added. It can be seen that the height bias is becoming the larger the larger the turbulence parameters. The same holds for its sigma. For the generation of the time series of equivalent turbulent zenith wet delays, the same 250 sets of random numbers were used, the differences thus being only due to the turbulence parameters (clock and white noise time series were also the same for every run). Summing up it can be said that the bias is influenced by i) the sequence of random numbers, ii) the turbulence parameters, and iii) the analysis strategy (not shown here). The sign of the bias is determined by i) and iii) while the turbulence parameters act as scaling parameters. Since always 16 stations are considered, this non-zero height bias should not be a problem but it is necessary to keep it in mind when interpreting results.

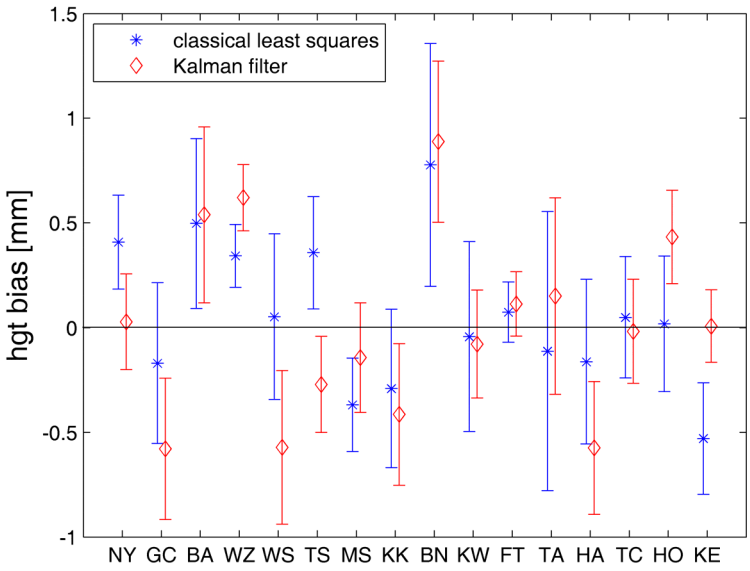

Figure 19: height biases in mm – blue: for a PPP with the classical least squares method (zwd: 6 min, 48 mm/h; grd: 6 min, 2 mm/h; clk: 1h, 54 mm/h), red: for a PPP with the Kalman filter (zwd: random walk, 0.7 ps²/s: grd: random walk, 0.5 ps²/s; clock: deterministic rate plus random walk offest, 1 ps²/s). The error bars show scatter/√25. The same time series of simulated group delay observables were used.

Finally, the investigations have shown that the observation density also has an impact on the choice of optimal parameters. Most of the simulations presented here were carried out for one and the same schedule. It has to be mentioned that the results might look slightly different when repeating the investigations for a schedule with a significantly different observation density.

In conclusion it has to be said that the results presented here do not always allow clear conclusions. The results should be interpreted very carefully, taking all these limitations into account. The findings presented here have to be confirmed with VLBI analysis software packages such as OCCAM and Calc/Solve. And, of course, these are just simulation studies. Although we consider the simulations to be the most realistic up to date, and although

comparisons of simulations to CONT05 real data (Wresnik et al., 2008, MacMillan, 2008) show good agreement, the strategies, even if confirmed with OCCAM and Calc/Solve, will have to be applied to real data as soon as possible to assess their benefit for future VLBI analyses.

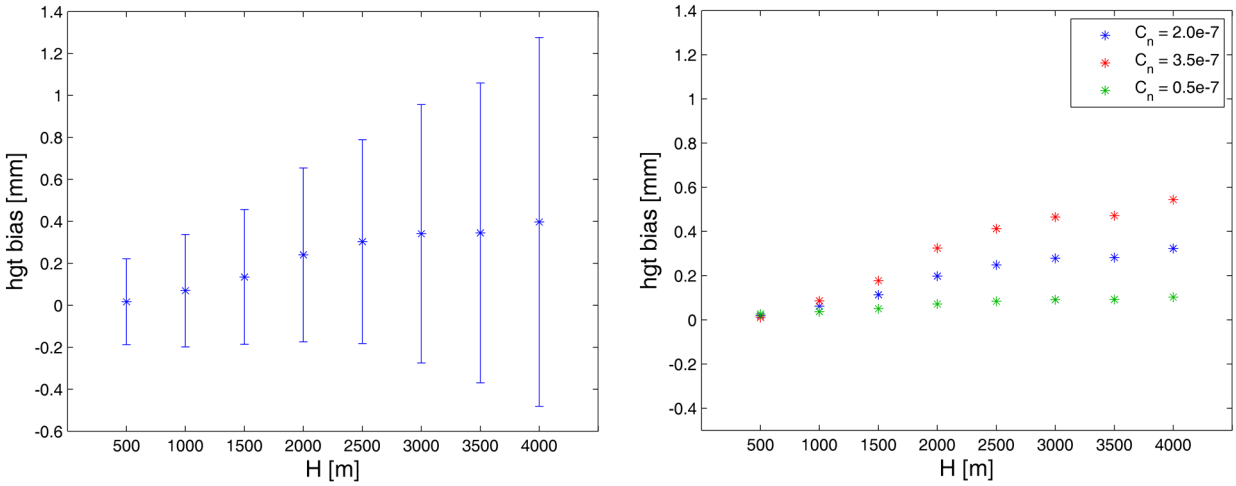

Figure 20: height biases for station WZ versus effective height of wet troposphere using the PPP Kalman filter. Left plot: C_n = 2.0e-7 $m^{-1/3}$, v = 7 m/s towards North-East, error bars show 1 sigma of the bias, i.e. scatter/√25; right plot: height biases for three different C_n values, v = 7 m/s towards North-East. Zwd: random walk, 0.7 ps²/s; gradients: random walk, 0.5 ps²/s; clk: deterministic rate plus random walk offset, 1 ps²/s. Schedule: st16uni_60_12_230X_0_0.skd; ASD 1e-14 @ 50 min; wn = 4/√2 ps. Always the same 250 sets of random numbers were used.

5. Summary

For both versions of the VLBI2010 PPP simulation software, the classical least squares version and the Kalman filter version, several parameters and strategies have been tested to assess their impact on position estimates. For the classical least squares method these were:

- rapid gradients,
- the impact of constraints,
- the length of estimation intervals, and
- elevation dependent weighting.

For the Kalman filter

- random walk gradients,
- the impact of variance rates, and
- elevation dependent weighting

were investigated.

It was found that the estimation of rapid gradients and random walk gradients respectively yields an improvement compared to the standard models (no gradients or slow gradients for the classical least squares, and no gradients or deterministic gradients for the Kalman filter). Another strategy that yielded promising improvement of 3D rms errors is elevation dependent weighting. It was shown that the impact of variance rates and constraints is either insignificant or at least pretty small.

The investigations have also shown that the optimal choice of parameters is mainly dependent on the prevailing atmospheric conditions and on the observation density making it impossible to come up with a general recommendation for a "best" parameterization. A good strategy for PPP solutions might be to use different parametrizations for dry and wet stations. Whether this might improve results of a network solution too, has to be tested. Nevertheless, it was shown that analyses strategies might have to be adapted to the new VLBI2010 schedules, mainly due to the increase in the number of observations, in order to gain the greatest benefit from this feature.

Appendix:

Most current set of turbulence parameters, provided by T. Nilsson from Onsala Space Observatory, used for the simulation studies presented here:

# ST	Cn	H	vnor	veas
#	[$m^{-1/3}$]	[m]	[m/s]	[m/s]
BA	0.83	2410	0.25	4.74
BN	3.09	1788	3.46	-2.20
FT	1.80	2459	2.93	-7.12
GC	0.55	2079	3.80	-6.49
HA	2.02	2450	2.03	-2.84
HO	1.15	1804	3.03	11.14
KE	0.93	2569	3.40	17.50
KK	2.28	1477	4.38	-3.36
KW	3.06	1477	-1.64	-9.42
MS	1.90	1322	7.64	0.91
NY	0.35	2173	7.46	0.53
TA	2.66	2006	5.45	-1.17
TC	1.40	1869	1.21	4.96
TS	1.44	1767	1.03	10.49
WS	1.16	2887	5.39	11.88
WZ	0.93	2040	6.75	4.22

References:

Behrend, D., J. Böhm, P. Charlot, T. Clark, B. Corey, J. Gispon, R. Haas, Y. Koyama, D. MacMillan, Z. Malkin, A. Niell, T. Nilsson, B. Petrachenko, A. Rogers, G. Tuccari, J. Wresnik, Recent Progress in the VLBI2010 Development, submitted to the proceedings of the IUGG General Assembly in Perugia, Italy, 2007

Böhm, J., H. Schuh, Spherical Harmonics as a Supplement to Global Tropospheric Mapping Functions and Horizontal Gradients, In: D. Behrend and A. Rius (Eds.): Proceedings of the 15th Working Meeting on European VLBI for Geodesy and Astrometry, Institut d'Estudis Espacials de Catalunya, Consejo Superior de Investigaciones Científicas, Barcelona, Spain, 143-148, 2001

Böhm, J., J. Wresnik, A. Pany, Simulation of wet zenith delays and clocks, IVS Memorandum 2006-013v03, 4 September 2007, ftp://ivscc.gsfc.nasa.gov/pub/memos/ivs-2006-013v03.pdf, 2007

Gipson, J., Incorporating Correlated Station Dependent Noise Improves VLBI Estimates, In: Proceedings of the 18th European VLBI for Geodesy and Astrometry Working Meeting, 12-13 April 2007, edited by J. Böhm, A. Pany and H. Schuh, Geowissenschaftliche Mitteilungen, Heft Nr. 79, Schriftenreihe der Studienrichtung Vermessung und Geoinformation, Technische Universität Wien, ISSN 1811-8380, 129-134, 2007

Herring, T., I. Shapiro, Geodesy by Radio Interferometry: The Application of Kalman Filtering to the Analysis of Very Long Baseline Interferometry Data, Journal of Geophysical Research, Vol. 95, No. B8, 12,561 – 12,581, 1990

MacMillan, D., VLBI2010 Simulations Using Solve, In: Proceedings of the 18th European VLBI for Geodesy and Astrometry Working Meeting, 12-13 April 2007, edited by J. Böhm, A. Pany and H. Schuh, Geowissenschaftliche Mitteilungen, Heft Nr. 79, Schriftenreihe der Studienrichtung Vermessung und Geoinformation, Technische Universität Wien, ISSN 1811-8380, 163-167, 2007

MacMillan, D., Comparisons of Observed and Simulated CONT05 Repeatabilities for Different Turbulence Cn Models, IVS Memorandum 2008-010v01, 22 July 2008, ftp://ivscc.gsfc.nasa.gov/pub/memos/ivs-2008-010v01.pdf, 2008

McCarthy, D., G. Petit, IERS Conventions 2003, Verlag des Bundesamtes für Kartographie und Geodäsie, Frankfurt am Main, 2004

Nilsson, T., R. Haas, G. Elgered, Simulations of atmospheric path delays using turbulence models, In: Proceedings of the 18th European VLBI for Geodesy and Astrometry Working Meeting, 12-13 April 2007, edited by J. Böhm, A. Pany and H. Schuh, Geowissenschaftliche Mitteilungen, Heft Nr. 79, Schriftenreihe der Studienrichtung Vermessung und Geoinformation, Technische Universität Wien, ISSN 1811-8380, 175-180, 2007

Pany, A.,J. Wresnik, J. Böhm, Vienna VLBI2010 PPP Simulator, IVS Memorandum 2008-012v01, 14 August 2008, ftp://ivscc.gsfc.nasa.gov/pub/memos/ivs-2008-012v01.pdf, 2008

Petrachenko, B., J. Böhm, D. MacMillan, A. Niell, A. Pany, A. Searle, J. Wresnik, VLBI2010 Antenna Slew Rate Study, submitted to the 5th IVS General Meeting Proceedings, 2008

Petrov, L., Using source maps for scheduling and data analysis: approaches and strategies, In: Proceedings of the 18th European VLBI for Geodesy and Astrometry Working Meeting, 12-13 April 2007, edited by J. Böhm, A. Pany and H. Schuh, Geowissenschaftliche Mitteilungen, Heft Nr. 79, Schriftenreihe der Studienrichtung Vermessung und Geoinformation, Technische Universität Wien, ISSN 1811-8380, 141-146, 2007

Vandenberg, N., NVI, Inc.: Interactive/Automatic Scheduling Program, Program Reference Manual, NASA/Goddard Space Flight Center, 1999

Wresnik, J., J. Böhm, A. Pany, H. Schuh, Towards a new VLBI system for geodesy and astrometry, Advances in Geosciences, AOGS 2007, accepted by the editor 2007

Wresnik, J., A. Pany, J. Böhm, Evaluation of the new Cn values for the turbulence model with CONT05 real data, IVS Memorandum 2008-044v01, 19 June 2008, ftp://ivscc.gsfc.nasa.gov/pub/memos/ivs-2008-004v01.pdf, 2008